Atmos. Chem. Phys., 25, 17387–17397, 2025 https://doi.org/10.5194/acp-25-17387-2025 © Author(s) 2025. This work is distributed under the Creative Commons Attribution 4.0 License.





Technical note: Apportionment of Southeast Asian biomass burning and urban influence via in situ trace gas enhancement ratios

Joshua P. DiGangi¹, Glenn S. Diskin¹, Subin Yoon^{2,a}, Sergio L. Alvarez², James H. Flynn², Claire E. Robinson^{1,3,8}, Michael A. Shook¹, K. Lee Thornhill^{1,3}, Edward L. Winstead^{1,3}, Luke D. Ziemba¹, Maria Obiminda L. Cambaliza^{4,5}, James B. Simpas^{4,5}, Miguel Ricardo A. Hilario⁶, and Armin Sorooshian⁶

¹NASA Langley Research Center, Hampton, VA 23681, USA

²University of Houston, Houston, TX 77204, USA

³Analytical Mechanics Associates, Inc., Hampton, VA 23666, USA

⁴Air Quality Dynamics Laboratory, Manila Observatory, Quezon City, 1101, Philippines

⁵Department of Physics, Ateneo de Manila University, Quezon City, 1101, Philippines

⁶University of Arizona, Tucson, AZ 85721, USA

^anow at: Scripps Institution of Oceanography, University of California San Diego, La Jolla, CA 92037, USA

⁸deceased

Correspondence: Joshua P. DiGangi (joshua.p.digangi@nasa.gov)

Received: 26 March 2025 – Discussion started: 14 May 2025 Revised: 29 August 2025 – Accepted: 8 September 2025 – Published: 2 December 2025

Abstract. Correlations in airborne in situ gas enhancement ratios of CH₄ to CO from the 2019 Cloud, Aerosol and Monsoon Processes Philippines Experiment (CAMP²Ex) field project over the Sulu, Philippine, and South China Seas were used to distinguish air masses with predominantly biomass burning, urban, or mixed influence, and identifying contributions from differing urban sources. Two approaches were created to produce a final data flag: one using a singular background for CO and CH₄ enhancement ratios and another determining enhancement ratios via linear regression of 4 min bins along the timeseries. HYSPLIT back trajectory analysis was used to identify air mass origins, and the resulting source regimes were examined for differences in ozone, reactive nitrogen, and aerosol chemical composition. $\Delta O_3/\Delta CO$ enhancement ratios were observed to be constant between urban source regimes, yet $\Delta NO_y/\Delta CO$ enhancement ratios differed across these regimes. For biomass burning sources, enhancement ratios in $\Delta O_3/\Delta CO$ were over a factor of two lower than those reported by previous studies in this region. Organic aerosol mass fractions were observed to be 2–3 times higher in biomass burning influenced regimes compared to urban regimes. This technique represents a simple yet powerful approach for separating emission influences in a chemically complex environment that enables identification and characterization of emission sources using exclusively routine measurements that can be accomplished with commonly available instrumentation.

1 Introduction

Biomass burning and urban fossil fuel emissions are both significant contributors to poor air quality. In particular, Southeast Asia is home to strong emissions of both types, and combined with many of the world's largest megacities, this contributes to widespread increased mortality due to respiratory diseases (Lee et al., 2018). Uncertainties in emissions and emission sources can exacerbate the difficulty in predicting these mortality effects (Marvin et al., 2024), thus improving the ability to accurately identify air mass emission sources, a crucial need to assist policymakers in crafting policies to reduce these premature deaths.

Back trajectory models have been utilized to great effect in identifying physical air mass histories (Fleming et al., 2012; Hilario et al., 2021, 2024; Robinson et al., 2011) but are limited by the resolution and accuracy of the assimilated meteorological information driving the model which can poorly represent sub-grid scale emissions and overestimate longrange transport (Harris et al., 2005). Gas tracer enhancement ratios, which exploit differing emission ratios, can provide a chemical ground truth at the measurement site (Halliday et al., 2019; Smith et al., 2015). While not providing an air mass physical history, the enhancement ratio can provide insight into the chemical history of the air mass, making it an excellent complement to back trajectory models. The choice of gas tracers depends on the application and time scale of the emissions and subsequent transport. Gases must either have similar chemical lifetimes to be viable or have a stable, known emission profile so that their differing lifetimes can be used as a chemical clock (Barmet et al., 2012; Gelencsér et al., 1997). For evaluating larger-scale regional or mesoscale emissions, relative enhancements in more stable tracers have been used to great effect (Plant et al., 2022). Commonly, enhancement ratios of carbon monoxide (CO) to carbon dioxide (CO₂) have been used to this end due to the direct relationship between their emission ratio and combustion efficiency (DiGangi et al., 2021; Halliday et al., 2019). However, this can be complicated in regions or seasons where biogenic or oceanic uptake of CO₂ can complicate the necessary stable tracer background (Silva et al., 2013).

In contrast, CO and methane (CH₄) are inefficiently scavenged by precipitation and cloud processes due to their low solubility, leaving dominant photochemical loss pathways typically on the order of many days to weeks for CO (Holloway et al., 2000; Khalil and Rasmussen, 1984) and years for CH₄ (Cicerone and Oremland, 1988; Naik et al., 2013; Voulgarakis et al., 2013), slow on the scale of regional or mesoscale transport. Thus, correlated enhancements between CO and CH₄ (Δ CH₄/ Δ CO) can be primarily related to the air mass source. Biomass burning has been widely reported in the literature to have low Δ CH₄/ Δ CO enhancement ratios or emission ratios compared to the higher values reported from fossil fuel combustion. For example, based on shipborne measurements in

the South China Sea while heavily influenced by biomass burning, Nara et al. (2017) reported a typical $\Delta CH_4/\Delta CO$ enhancement ratio of $7.95\pm0.21\,\%$ ppb ppb $^{-1}$. Worden et al. (2017) report biomass burning $\Delta CH_4/\Delta CO$ emission ratios between $0\,\%$ ppb ppb $^{-1}$ and $20\,\%$ ppb ppb $^{-1}$ over a variety of global domains based on Aura TES retrievals and GFED-driven GEOS-Chem modeling. In contrast, Helfter et al. (2016) observed CH₄/CO flux emission ratios between $60\,\%$ – $500\,\%$ during urban eddy covariance flux studies over central London, UK, and Plant et al. (2019) observed mean $\Delta CH_4/\Delta CO$ enhancement ratios between 48 % ppb ppb $^{-1}$ and 130 % ppb ppb $^{-1}$ from airborne studies over six Eastern US cities.

We present a new approach that combines multiple methods for calculating enhancement ratios of $\Delta CH_4/\Delta CO$ to isolate contributions from differing chemical regimes observed during the 2019 Clouds, Aerosol and Monsoon Processes-Philippines Experiment (CAMP²Ex) field campaign. These chemical regimes were then compared with those determined through back trajectory analysis to corroborate the expected source regimes and predict their emission origin. Finally, the regimes were used to examine contributors to poor air quality (ozone, reactive nitrogen, aerosol) by attributed source.

2 Methods

2.1 CAMP²Ex

CAMP²Ex was a joint field campaign sponsored by NASA, the Naval Research Laboratory, and the Manila Observatory in 2019 based in the Philippines (Reid et al., 2023), which predominantly sampled air masses over the Sulu, Philippine, and South China Seas (Fig. S1 in the Supplement). The overarching science questions were focused on improving understanding of the coupling of aerosol, cloud, and radiation processes in a complex chemical and meteorological environment. The measurement platforms included two aircraft, the NASA P-3 and the SPEC Learjet 35 based at Clark International Airport in Luzon, the Scripps R/V Sally Ride stationed in the Philippine Sea, and a ground station at Manila Observatory inside the Ateneo de Manila University in Quezon City, Metro Manila. Flight profiles ranged over the South China, Philippine, and Sulu Seas, capturing a variety of compositional and cloud environments (Hilario et al., 2021). The P-3 aircraft fielded a comprehensive payload, with a mixture of remote sensing and in situ cloud, aerosol, and composition instrumentation, data from which are the focus of this study. All flight data presented in this work are from P-3 in situ data averaged on a 5 s time base (i.e., a 5 s data merge), and all data are publicly available (NASA/LARC/SD/ASDC, 2020). These measurements sampled a variety of pollution sources during both the southwest monsoon and monsoon transition periods and provided an opportunity to examine how local and transported emissions affected air mass chemical composition and air quality.

2.2 Measurements

Gas phase CO₂, CH₄, and CO dry mole fractions were collected at 0.4 Hz resolution via a commercial near-infrared cavity ringdown spectrometer (G2401-m: Picarro, Inc.) fitted with a custom airborne sampling system to increase stability and reduce sampling artifacts (DiGangi et al., 2021). Two-point calibrations were performed hourly during flight using standards prepared by NOAA ESRL and traceable to the WMO X2007 (CO₂), X2004A (CH₄), and X2014A (CO) scales. Precisions for CO₂, CH₄, and CO during CAMP²Ex were 0.1 ppm, 1 ppb, and 5 ppb, and accuracies were 0.1 ppm, 1 ppb, and 2 %, respectively. Ozone (O₃) was measured using a pair of commercial dual-beam UV absorption sensors (Model 205: 2B Technologies, Inc.) fitted with a custom sampling manifold to enhance high altitude performance (Wei et al., 2021). Calibrations were performed in the laboratory prior to the campaign using a commercial NIST-traceable ozone generator (Model 306: 2B Technologies, Inc.). Due to an altitude-dependent discrepancy between the two sensors, final ozone data were reported as the average of the two measurements, with a combined uncertainty of 6 % from both the intercomparison and the native uncertainty of the instrument.

Water vapor mixing ratios were measured via open-path near infrared absorption spectroscopy by the NASA Diode Laser Hygrometer (Diskin et al., 2002). Nitrogen oxide (NO), summed total NO + nitrogen dioxide (NO₂) (NO + $NO_2 = NO_x$), and total reactive nitrogen (NO_y) were measured using a two-channel chemiluminescence nitrogen oxide analyzer (Air Quality Design Inc.) sampling through an unheated PFA-sheathed inlet. NO and NOx were sampled serially on one channel using a 395 nm UV LED photolytic NO₂ converter (Air Quality Design Inc.). A molybdenum converter operating at 300 °C mounted near the sample entry point to the aircraft cabin was used to convert NO_{ν} species to NO for detection. The NO, NO_2 , and NO_{ν} limit of detection was 0.30, 0.27, 0.22 ppb with an uncertainty of 12 %, 14 %, and 12 %, respectively. Submicron nonrefractory aerosol mass concentrations were measured using a High-Resolution Time-of-Flight Aerosol Mass Spectrometer (HR-ToF-AMS, Aerodyne Research, Inc.) using standard data processing methods (Canagaratna et al., 2007; De-Carlo et al., 2006). HR-ToF-AMS measurements were obtained behind a pressure-controlled inlet for stability and were recorded in FastMS mode (25 s open, 5 s closed) and averaged to approximately 30 s for this analysis. Mass concentrations are reported at standard temperature and pressure (273 K and 1013.25 hPa), and sulfate, nitrate, ammonium, chlorine, and organic mass concentrations were determined using standard fragmentation tables (Allan et al., 2004). In this analysis, total AMS aerosol mass is defined as the sum of each of these five AMS species contributions.

3 Emission Flag Derivation

To separate out different chemical regimes observed in the CAMP²Ex dataset, specifically biomass burning versus urban emissions, this work leverages differences in the populations of enhancement ratios of CH₄ and CO. A combination of two different approaches to calculating Δ CH₄/ Δ CO enhancement ratios was used to isolate the biomass burning and urban regimes: one using a single campaign background to determine enhancement ratios (Sect. 3.1) and a second using dynamic linear fitting on a rolling time window throughout each flight to find correlated enhancement ratios (Sect. 3.2). The final flag merging these approaches was calculated for each timestamp in the 5 s data merge (Sect. 3.4).

3.1 Single Background Approach

The single background approach centers around the use of single background concentrations of CO and CH₄ for the purpose of calculating mixing ratios. Conceptually, this approach assumes that emitted air is broadly mixing exclusively with some idealized regional background air. To determine these ideal background concentrations, subsets of data at high enhancement ratios were chosen that appeared to represent individual mixing lines and fit with a simple least squares linear regression. The most common intersection of these fits was chosen as the assigned background concentrations, which was 65 ppb for CO and 1.85 ppm for CH₄. However, much of the data at small CH₄ and/or CO enhancements above these background levels were still not separable into urban and biomass burning regimes due to variability of the true background concentration of each species. Thus, it was necessary to find the minimum ΔCH_4 and ΔCO enhancement above background at which the two regimes begin to be separable while also as low as possible to maximize the data capable of being assigned to each regime. To accomplish this, the frequency distribution of $\Delta CH_4/\Delta CO$ enhancement ratios were examined at various ΔCH_4 and ΔCO enhancement levels above background concentrations (Fig. 1a-b). In these plots, the high data frequency peaks of both the biomass burning regime (at low $\Delta CH_4/\Delta CO$ enhancement ratios) and the urban regime (at high $\Delta CH_4/\Delta CO$ enhancement ratios) appear as high peaks off scale. As the cutoff enhancement concentrations were increased, a minimum in the frequency distribution emerges between 35 % ppb ppb $^{-1}$ and 70 % ppb ppb⁻¹ Δ CH₄/ Δ CO (Fig. 1a–b, grey shaded area). The cutoff concentration enhancements at which this minimum emerges were determined to be the minimum enhancement at which the urban and BB data populations could be isolated: 40 ppb for ΔCH_4 and 55 ppb for ΔCO . Once the cutoff concentration was reached in the CO or CH4 time series, a deadband of an additional Δ10 ppb CO and CH₄ was added to avoid rapid regime switching influenced by instrument precision limitations, an example of which is shown in Fig. S2. Flag categories were then assigned by enhancement

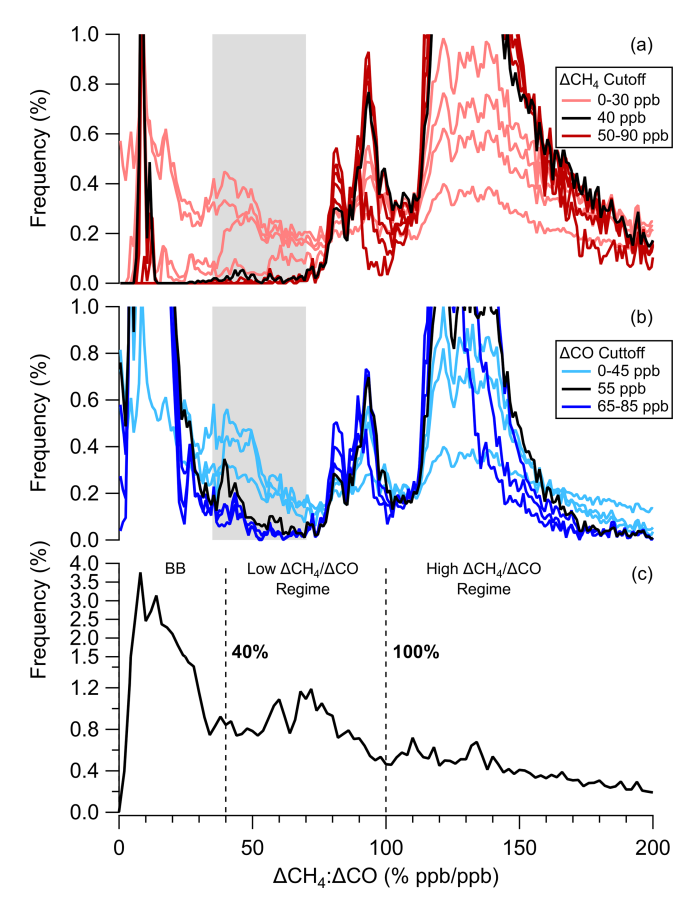


Figure 1. Sensitivity test of $\Delta \text{CH}_4/\Delta \text{CO}$ emission ratio distributions to concentration cutoffs in (a) CH₄ and (b) CO. Shaded area shows the minimum in $\Delta \text{CH}_4/\Delta \text{CO}$ chosen to separate the regimes above the selected cutoffs at $\Delta \text{CH}_4 = 40 \text{ ppb}$ and $\Delta \text{CO} = 55 \text{ ppb}$. (c) Frequency distribution of $\Delta \text{CH}_4/\Delta \text{CO}$ enhancement ratios showing rolling slope regimes, with dashed lines representing the slope cutoffs between regimes at 40 % and 100 % $\Delta \text{CH}_4/\Delta \text{CO}$.

ratio and intensity of enhancement with respect to these cutoff concentrations (Fig. 2a).

3.2 Rolling Slope Approach

As the single background technique is limited due to the coarse assumption of a constant chemical background over the entirety of the campaign, a different approach was used to extract more fine detailed information from the dataset. With this approach, the linear fits of CH₄ vs. CO were calculated using weighted orthogonal distance regression (ODRPACK95 – IGOR Pro v7; Wu and Yu, 2018) for 4 min rolling windows through each flight, similar to the technique used by Halliday et al. (2019) and DiGangi et al. (2021) for Δ CO/ Δ CO₂ enhancement ratios. Rolling windows with lower goodness of fit (r^2 < 0.5) were filtered as uncorrelated. Slopes from the remaining fits represent a Δ CH₄/ Δ CO enhancement ratio product that is independent of changes in larger scale shifts in background concentra-

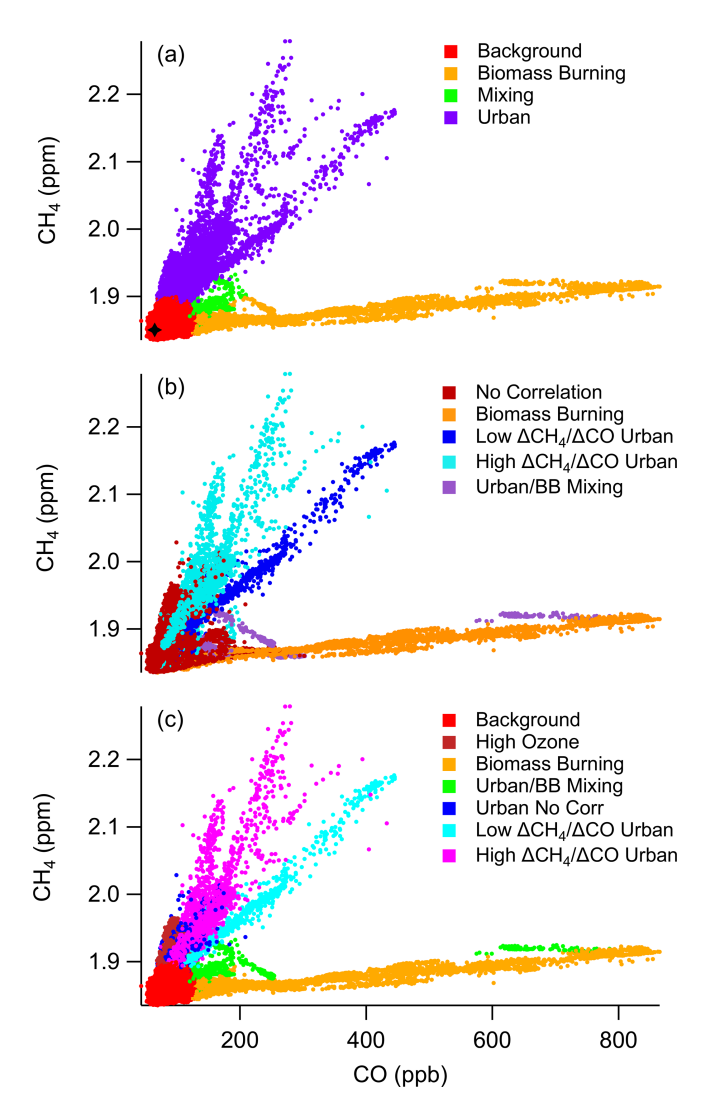


Figure 2. Tracer correlation plot of CH₄ vs. CO mole fractions colored by regime excluding Clark-influenced data using the (a) single background method (black star denotes background values), (b) rolling slope method, (c) final combined method.

tion and more sensitive to mixing from recent emissions. In the frequency distribution of the $\Delta CH_4/\Delta CO$ slopes, three relative minima in the frequency distribution (Fig. 1c) were chosen to separate the dataset into four regimes (Table 1). One is a negative-slope regime that corresponded to mixing between urban-influenced and biomass burning-influenced air. A second regime was between $0\,\%$ ppb ppb $^{-1}$ and $40\,\%$ ppb ppb $^{-1}$ $\Delta CH_4/\Delta CO$, peaking near $10\,\%$ ppb ppb $^{-1}$ and $40\,\%$ ppb ppb $^{-1}$ $\Delta CH_4/\Delta CO$, with low slopes corresponding to biomass burning. The last two regimes had higher slopes consistent with urban influence: a moderate slope regime between $40\,\%$ ppb ppb $^{-1}$ and $100\,\%$ ppb ppb $^{-1}$ $\Delta CH_4/\Delta CO$, peaking around $60\,\%$ ppb ppb $^{-1}$ and $80\,\%$ ppb ppb $^{-1}$ $\Delta CH_4/\Delta CO$, and a higher sloped regime containing slopes above $100\,\%$ ppb ppb $^{-1}$ $\Delta CH_4/\Delta CO$ with a broad, multifea-

tured peak near the range of $110\,\%$ ppb ppb $^{-1}$ through $140\,\%$ ppb ppb $^{-1}$ and a long tail toward higher $\Delta CH_4/\Delta CO$ slopes. Finally, the resulting flag was manually filtered to merge clearly temporally contiguous air masses that may only have had correlation over a portion of the sampling region (Fig. 2b).

3.3 Special Cases

Data influenced by strong local sources during takeoff at Clark International Airport were flagged separately until the first sharp gradient in trace gas concentration/humidity or, if no gradient was discernible, until 1 km above ground level (a.g.l.). Similarly, Clark influence prior to landing was flagged as either the last sharp trace gas concentration/humidity gradient or 1 km a.g.l. through the end of the flight. A separate population of data was flagged as another special case shown in Fig. S3, where a lobe in the $\Delta CH_4/\Delta CO$ scatterplot (Fig. S3a) was identified due to a strong anticorrelation between ozone and water vapor data (Fig. S3b) at low water mixing ratios (< 8000 ppm_v). This may be indicative of stratospheric mixing (Pan et al., 2014), which would normally also result in anti-correlations between ozone and both CH₄ and CO (Collins et al., 1993; Pan et al., 2004). In contrast, these ozone observations are uncorrelated with CO and appear positively correlated with CH₄ (Fig. S3cd, respectively), analysis of which is deemed beyond the scope of this work. As these two cases are distinct from the rest of the dataset, both the Clark-influenced and potential stratospherically-influenced data were flagged as separate values in the data product and neglected in further analysis.

3.4 Final Combined Flag

The final flag background and biomass burning regimes were equivalent to those assigned by the single background method. The urban regime from the single background method was split into three separate regimes based on the correlated slope (or lack thereof) from the rolling slope method. The negative-slope correlated regime was combined with the urban/BB mixing regime from the single background method to form the final urban/biomass burning mixing regime. Figure 2c shows the final regime apportionments with respect to CH₄ and CO, while Table 1 shows the final cutoffs in both tracer enhancement and enhancement ratios for each method.

4 Discussion

4.1 HYSPLIT Back Trajectory Comparison

To evaluate the utility of the emission flag and assign potential origins of the empirically-derived populations, hourly back trajectories were calculated using the NOAA Hybrid

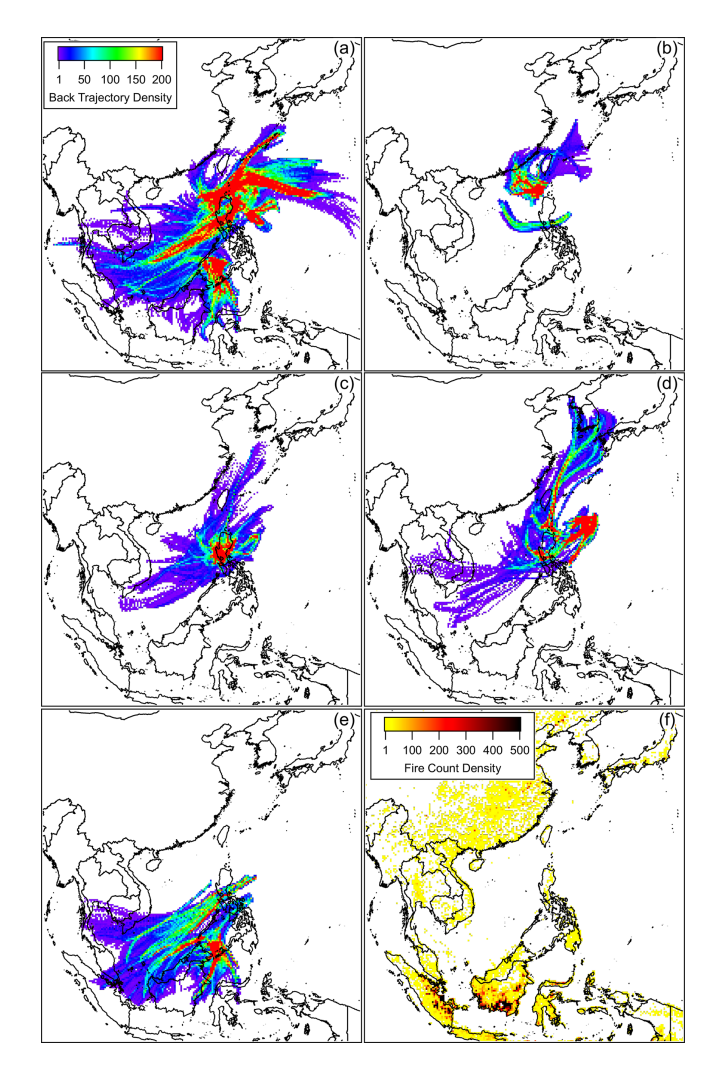


Figure 3. Heat map of HYSPLIT 48 h back trajectories at 1 h resolution initialized every 5 s from flight track < 2 km, separated by regime: (a) background, (b) low $\Delta CH_4/\Delta CO$ urban, (c) high $\Delta CH_4/\Delta CO$ urban, (d) uncorrelated urban, and (e) biomass burning. (f) Heat map of VIIRS 375 m fire counts during September 2019.

Single Particle Lagrangian Integrated Trajectory (HYSPLIT) model (Rolph et al., 2017; Stein et al., 2015), similar to those described in Hilario et al. (2021). Aircraft latitude, longitude, and altitude from the P-3 data merge were used to initialize the model for each 5 s point along the flight track for all flights. The Global Forecast System (GFS) 0.25° resolution reanalysis product from the National Centers for Environmental Protection (NCEP) was used to drive the modeled meteorology. Figure 3 shows a summary of heat maps of the resulting hourly back trajectory points under 2 km above mean sea level, an altitude cutoff intended to isolate contributions to the back trajectories originating from the planetary boundary layer. Data were binned to 0.25° resolution where the bin color denotes the frequency of a contribution. Each heat map

Regime	Single Background		Rolling Slope
	Enhancement Cutoff	Enhancement Ratio Cutoff (ppb ppb ⁻¹)	$\Delta CH_4/\Delta CO \text{ Limits}$ $(ppb ppb^{-1})$
Urban/Biomass Burning Mixing	Δ CO < 55 ppb Δ CH ₄ < 40 ppb	_	$\Delta CH_4/\Delta CO < 0\%$
Biomass Burning	$\Delta CO > 55 \text{ ppb}$	$\Delta \text{CH}_4/\Delta \text{CO} < 35\%$	$0\% < \Delta CH_4/\Delta CO < 40\%$
Urban Low $\Delta CH_4/\Delta CO$ Regime	$\Delta CO > 55 \text{ ppb } \Delta CH_4 > 40 \text{ ppb}$	$35\% < \Delta CH_4/\Delta CO < 70\%$	$40\% < \Delta CH_4/\Delta CO < 100\%$
Urban High $\Delta CH_4/\Delta CO$ Regime	$\Delta \text{CH}_4 > 40 \text{ ppb}$	$\Delta \text{CH}_4/\Delta \text{CO} > 70 \%$	$\Delta \text{CH}_4/\Delta \text{CO} > 100 \%$

Table 1. Cutoff concentration enhancements for CO and CH₄ for both single and rolling slope background methods.

represents back trajectories initialized during a different observed chemical regime.

Trajectories observed from the background chemical regime (Fig. 3a) were well dispersed around the region, though few back trajectories appear over land in the boundary layer within the 48 h time window. In contrast, trajectories observed during the biomass burning chemical regime (Fig. 3b) were focused toward the southwest of the flight domain. The bulk of these were focused from the direction of Borneo and Sulawesi, though contributions appear from as far as Sumatra, the Malay peninsula, and the rest of mainland Southeast Asia. These results were consistent with the larger clusters in September 2019 observed fire counts (Fig. 3f) from the VIIRS 375 m product (NASA FIRMS, 2020). Of the correlated urban regimes, the low $\Delta CH_4/\Delta CO$ urban regime back trajectories (Fig. 3c) were predominantly either from over continental China or from that direction. The high $\Delta CH_4/\Delta CO$ urban regime was observed more frequently and appears from the back trajectories (Fig. 3d) to be focused locally in and around Luzon. The most frequent contributions in the uncorrelated urban regime (Fig. 3e) seemed to originate from Korea and Kyushu (Japan), the distance from which could be an explanation for existence of consistent CO and CH₄ enhancements with no short-term correlations between the species. The partitioning of the back trajectories was based only on the $\Delta CH_4/\Delta CO$ -derived chemical regimes, yet results in distinct separation in the back trajectory regimes, providing evidence toward the validity of this technique.

4.2 Ozone and Reactive Nitrogen Regime Dependencies

The ozone and reactive nitrogen measurements can give insight into the relative contributions within the different chemical regimes observed during the campaign. Figure 4a shows enhancements in ozone with respect to CO for each regime. Biomass burning $\Delta O_3/\Delta CO$ is very strongly correlated (r^2 0.93) with a slope of 7.6 \pm 0.3% ppbv ppb $^{-1}$, which is lower than both the 18 ± 8 % ppbv ppb $^{-1}$ reported by Lin et al. (2013) and the 20 ± 1 % ppbv ppbv $^{-1}$ reported by Kondo et al. (2004) in roughly the same region. Seasonality may affect these results somewhat, as the Lin et

al. (2013) measurement values represent an annual range and the Kondo et al. (2004) values were only during February-April, both contrasting with the measurements exclusively during August-October in this work. Otherwise, this may be indicative of a change in emission patterns over the previous decade, with lower O_3 production implying different NO_x or VOC loading. Urban $\Delta O_3/\Delta CO$ enhancements from all categories were not readily separable, but taken as one, they were still well correlated (r^2 0.71) with a slope of $35 \pm 2\%$ ppbv ppb⁻¹.

This consistency in $\Delta O_3/\Delta CO$ correlations among the urban regimes did not persist for the reactive nitrogen/CO ratios. $\Delta NO_v/\Delta CO$ enhancements were used to represent reactive nitrogen enhancements in the different regimes, as shown in Fig. 4b. Biomass burning $\Delta NO_v/\Delta CO$ was not as correlated as $\Delta O_3/\Delta CO$ with an r^2 of 0.45 and a slope of 0.144 ± 0.002 pptv ppb⁻¹. $\Delta NO_v/\Delta CO$ enhancements were similarly correlated in the high and low $\Delta CH_4/\Delta CO$ urban regimes with r^2 values of 0.33 and 0.38, respectively. However, in contrast with the $\Delta O_3/\Delta CO$ urban correlations, the high and low $\Delta CH_4/\Delta CO$ urban regimes exhibited distinctive $\Delta NO_v/\Delta CO$ slopes, with the high $\Delta \text{CH}_4/\Delta \text{CO}$ regime slope $(8.7 \pm 0.2 \text{ pptv ppb}^{-1})$ a factor of six greater than the low $\Delta CH_4/\Delta CO$ urban regime slope $(1.38 \pm 0.02 \,\mathrm{pptv}\,\mathrm{ppb}^{-1})$. This range of ratios is comparable to those reported by Kondo et al. (2004), who observed $\Delta NO_y/\Delta CO$ slopes of 2.2 ± 0.6 pptv ppbv⁻¹ in the planetary boundary layer and $7.9 \pm 0.3 \,\mathrm{pptv}\,\mathrm{ppbv}^{-1}$ in the lower troposphere over Southeast Asia in primarily urbaninfluenced air during TRACE-P in 2001. In general, higher NO_v/CO emission factors are indicative of higher efficiency combustion, as high temperatures lead to both more complete conversion of carbon to CO_2 and greater NO_x production. This would infer that urban combustion sources sampled in the high $\Delta CH_4/\Delta CO$ regime were on average more efficient than those sampled in the low $\Delta CH_4/\Delta CO$ regime. More broadly, the common ozone dependency under these drastically different reactive nitrogen environments suggests that ozone production in the low and high $\Delta CH_4/\Delta CO$ urban regimes may have been VOC-limited.

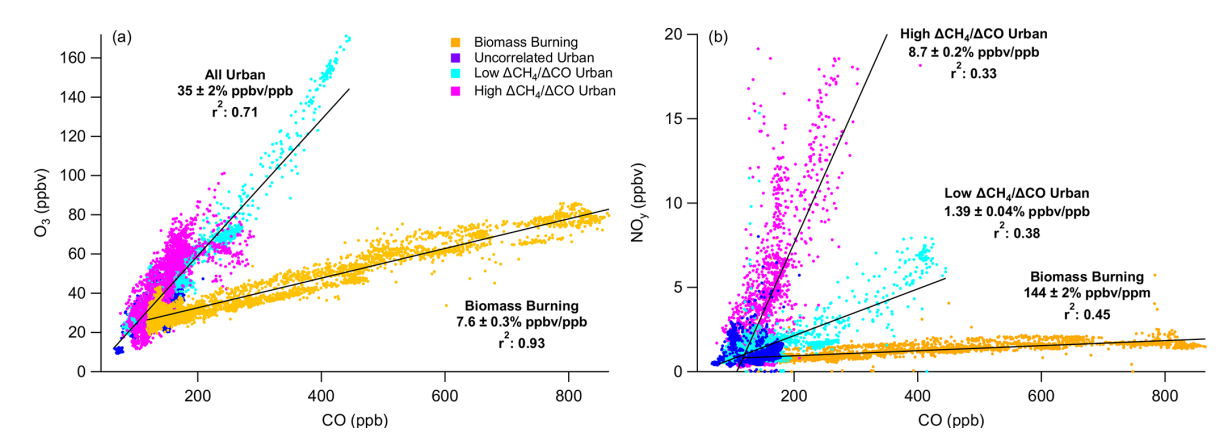


Figure 4. Tracer-tracer plots of (a) O_3 and (b) NO_y versus CO separated by chemical regime. Trend lines denote linear fits for their respective regimes.

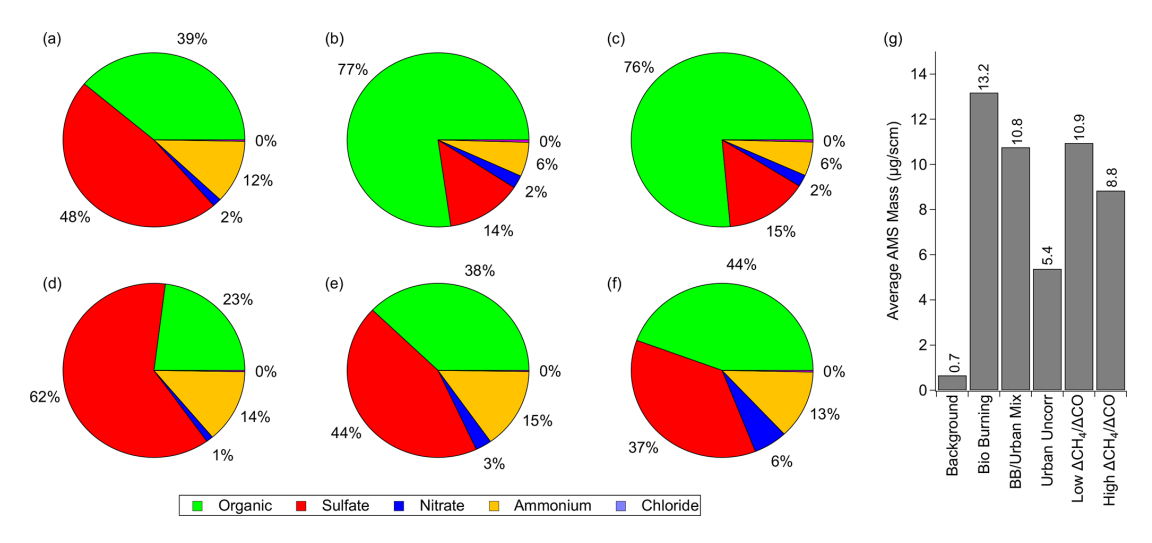


Figure 5. Relative aerosol chemical composition with respect to chemical regime: (a) background, (b) biomass burning, (c) biomass burning/urban mixing, (d) uncorrelated urban, (e) low $\Delta CH_4/\Delta CO$ urban, (f) high $\Delta CH_4/\Delta CO$ urban. (g) Average total AMS mass concentration by regime.

4.3 Aerosol Composition Regime Dependencies

To evaluate the chemical regime effects on aerosol composition, Fig. 5a-f shows the relative speciated contribution to aerosol mass observed by the AMS in each regime integrated over the entire campaign, while Fig. 5g shows the total aerosol mass observed in each regime, also over the entire campaign. The biomass burning regime (Fig. 5b) exhibited the highest average aerosol mass concentration ($13 \mu g m^{-3}$) and the largest relative mass contribution from organic aerosols (77%). The BB/urban mixing regime (Fig. 5c) exhibited nearly identical relative aerosol contributions to the biomass burning regime, likely related to the observed larger mass loading from biomass burning compared to urban emissions. Among the urban regimes, the highest average mass concentration was observed in the low $\Delta CH_4/\Delta CO$ urban regime ($11 \,\mu g \,m^{-3}$), with relative aerosol contributions very similar to those observed in the background regime: \sim 40 %

each organic and sulfate aerosol mass. The high $\Delta CH_4/\Delta CO$ urban regime exhibited less aerosol on average $(8.8 \,\mu g \,m^{-3})$ than the low $\Delta CH_4/\Delta CO$ urban regime (10.9 µg m⁻³) and had very similar composition with also $\sim 40\%$ each organic and sulfate aerosol mass. In the background regime (Fig. 5a), average aerosol loading was much lower ($\sim 0.7 \,\mu \mathrm{g}\,\mathrm{m}^{-3}$) than for other regimes, and the largest relative contribution was from sulfate aerosols, with 49 % of the loading, followed by organic aerosols for another 39 %. In contrast, the biomass burning (Fig. 5b) and BB/urban (Fig. 5c) mixing regimes had similar relative mass contributions with respectively 77 % and 76% of the observed aerosol mass contribution from organic aerosol and only about 14% and 15% respectively from sulfate aerosol. Between the urban regimes, the uncorrelated regime had the lowest average aerosol mass but a larger relative sulfate aerosol contribution (62 %) compared

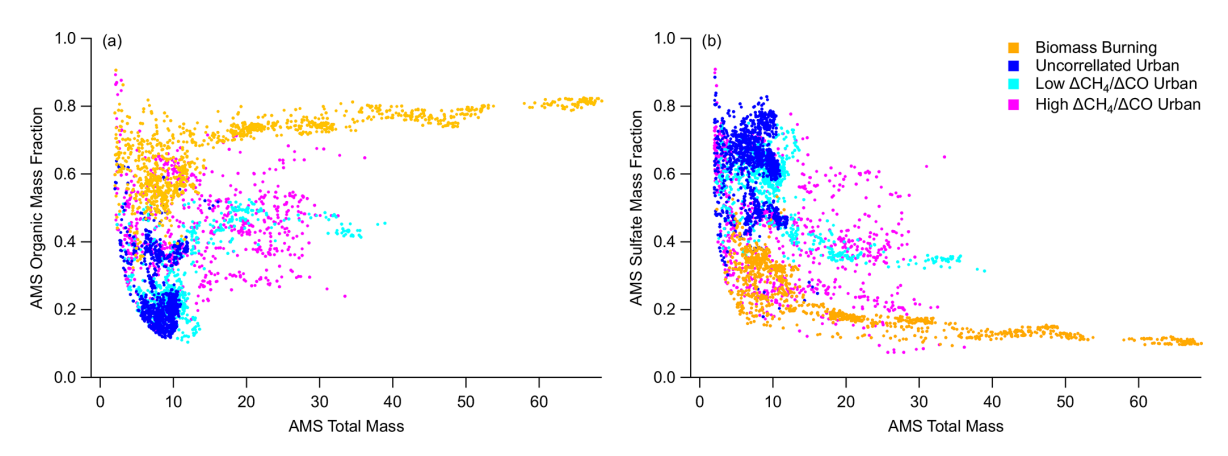


Figure 6. Relative AMS mass fractions of (a) organics and (b) sulfates versus total AMS mass concentration by chemical regime.

to the low and high $\Delta CH_4/\Delta CO$ urban regimes (44% and 37% respectively).

Figure 6 shows the trend in relative mass fraction contributions for the two dominant aerosol mass contributors, organic and sulfate, as a function of total aerosol mass in the biomass burning and urban chemical regimes. Within the urban regimes, there was large variability in the mass fractions for both organic and sulfate. One exception seems to be that the mass fractions asymptote at nearly 50 % (organic) and 35 % (sulfate) of total aerosol mass within the low $\Delta CH_4/\Delta CO$ urban regime, though this could be an example of the more limited observations of this regime. In the biomass burning regime, the mass fractions have high total mass asymptotes near 80 % (organic) and 10 % (sulfate).

5 Summary

Enhancement ratios in airborne in situ CH₄ and CO were used to isolate predominant sources of air mass emission influence during the CAMP²Ex campaign over the western Pacific near the Philippines. Due to a more variable background in CO₂ during CAMP²Ex, Δ CH₄/ Δ CO was observed to exhibit greater utility in discerning combustion emission sources in comparison to the more commonly used $\Delta CO/\Delta CO_2$, a metric of combustion efficiency. A 5 s data product was derived for all flights assigning regimes of biomass burning and various urban sources based on natural groupings of ranges of ΔCH₄/ΔCO enhancement ratios. HYSPLIT back trajectory modeling was used to predict the likely emission origins of the differing regimes and to corroborate the method, with a higher $\Delta CH_4/\Delta CO$ corresponding to local emissions and a lower $\Delta CH_4/\Delta CO$ corresponding to continental outflow. $\Delta O_3/\Delta CO$ were individually strongly correlated in both biomass burning and urban regimes, but with a much lower slope for biomass burning $(7.6 \pm 0.3 \% \text{ ppbv ppb}^{-1})$ compared to the slope for combined urban regimes $(35 \pm 2\% \text{ ppbv ppb}^{-1})$. $\Delta NO_{\nu}/\Delta CO$ were also highly correlated but had a sixfold higher slope for the local high $\Delta CH_4/\Delta CO$ urban regime compared to the continental outflow low $\Delta CH_4/\Delta CO$ urban regime. Organic aerosols were observed to dominate aerosol mass fractions for biomass burning influenced regimes at ~ 75 % of the total mass fraction, whereas background as well as low and high $\Delta CH_4/\Delta CO$ urban regimes were more evenly balanced between sulfate and organic aerosols.

The multi-faceted method developed in this analysis provides a novel approach to assessing regional source contributions. One caveat is that this method appears to work well at receptor sites away from direct sources as in CAMP²Ex but may not work as well very close to emission sources or in air masses simultaneously influenced by both biomass burning and fossil fuel combustion. The use of these simple tracer relationships perhaps achieved using common, commercially-available instrumentation, may provide a feasible approach for constraining certain emission sources without requiring the cost and complexity of a larger-scale experimental effort. Thus, this method can more broadly assist scientists and policymakers in understanding the impact of emission type on air quality metrics, particularly in regions where data from more complex instrumentation (e.g. PTR-MS, GC) are sparse.

CAMP²Ex Data availability. All airborne data is available from NASA on the project data archive https://doi.org/10.5067/SUBORBITAL/CAMP2EX2018/DATA001 (NASA/LARC/SD/ASDC, 2020). The **HYSPLIT** is a product of NOAA and available at https://www. ready.noaa.gov/HYSPLIT.php 29 (last access: April 2021). VIIRS fire count data is available from NASA at https://doi.org/10.5067/FIRMS/VIIRS/VNP14IMGT_NRT.002 (NASA FIRMS, 2020).

Supplement. The supplement related to this article is available online at https://doi.org/10.5194/acp-25-17387-2025-supplement.

Author contributions. JPD, GSD, SY, SLA, JHF, CER, MAS, KLT, ELW, and LDZ participated in the data collection. JPD, GSD, LDZ, MOLC, JBS, MRAH, and AS performed the data analysis and provided feedback. JPD prepared the manuscript with contributions from all coauthors.

Competing interests. At least one of the (co-)authors is a member of the editorial board of *Atmospheric Chemistry and Physics*. The peer-review process was guided by an independent editor, and the authors also have no other competing interests to declare.

Disclaimer. Publisher's note: Copernicus Publications remains neutral with regard to jurisdictional claims made in the text, published maps, institutional affiliations, or any other geographical representation in this paper. While Copernicus Publications makes every effort to include appropriate place names, the final responsibility lies with the authors. Also, please note that this paper has not received English language copy-editing. Views expressed in the text are those of the authors and do not necessarily reflect the views of the publisher.

Acknowledgements. The authors thank NASA, the Naval Research Laboratory, and Manila Observatory for their support. Thanks to Mario Rana of Analytical Mechanics Associates, Inc. as well as Jim Plant and Jimmy Geiger from NASA for their technical assistance. The authors gratefully acknowledge the NOAA Air Resources Laboratory (ARL) for the provision of the HYSPLIT transport and dispersion model and READY website (https://www.ready.noaa.gov, last access: 29 April 2021) used in this publication. We acknowledge the use of data and/or imagery from NASA's Fire Information for Resource Management System (FIRMS) (https://earthdata.nasa.gov/firms, last access: 28 January 2025), part of NASA's Earth Observing System Data and Information System (EOSDIS). University of Arizona investigators were supported by NASA grant 80NSSC18K0148 in support of CAMP²Ex.

Financial support. This research has been supported by the National Aeronautics and Space Administration (grant no. 80NSSC18K0148).

Review statement. This paper was edited by Benjamin A Nault and reviewed by two anonymous referees.

References

Allan, J. D., Delia, A. E., Coe, H., Bower, K. N., Alfarra, M. R., Jimenez, J. L., Middlebrook, A. M., Drewnick, F., Onasch, T. B., Canagaratna, M. R., Jayne, J. T., and Worsnop, D. R.: A generalised method for the extraction of chemically resolved mass spectra from Aerodyne aerosol mass spectrometer data, J. Aerosol Sci., 35, 909–922, https://doi.org/10.1016/j.jaerosci.2004.02.007, 2004.

- Barmet, P., Dommen, J., DeCarlo, P. F., Tritscher, T., Praplan, A. P., Platt, S. M., Prévôt, A. S. H., Donahue, N. M., and Baltensperger, U.: OH clock determination by proton transfer reaction mass spectrometry at an environmental chamber, Atmos. Meas. Tech., 5, 647–656, https://doi.org/10.5194/amt-5-647-2012, 2012.
- Canagaratna, M. R., Jayne, J. T., Jimenez, J. L., Allan, J. D., Alfarra, M. R., Zhang, Q., Onasch, T. B., Drewnick, F., Coe, H., Middlebrook, A., Delia, A., Williams, L. R., Trimborn, A. M., Northway, M. J., DeCarlo, P. F., Kolb, C. E., Davidovits, P., and Worsnop, D. R.: Chemical and microphysical characterization of ambient aerosols with the aerodyne aerosol mass spectrometer, Mass Spectrom. Rev., 26, 185–222, https://doi.org/10.1002/mas.20115, 2007.
- Cicerone, R. J. and Oremland, R. S.: Biogeochemical aspects of atmospheric methane, Global Biogeochem. Cy., 2, 299–327, https://doi.org/10.1029/GB002i004p00299, 1988.
- Collins Jr., J. E., Sachse, G. W., Anderson, B. E., Weinheimer, A. J., Walega, J. G., and Ridley, B. A.: AASE-II in-situ tracer correlations of methane, nitrous oxide, and ozone as observed aboard the DC-8, Geophys. Res. Lett., 20, 2543–2546, https://doi.org/10.1029/93GL02624, 1993.
- DeCarlo, P. F., Kimmel, J. R., Trimborn, A., Northway, M. J., Jayne, J. T., Aiken, A. C., Gonin, M., Fuhrer, K., Horvath, T., Docherty, K. S., Worsnop, D. R., and Jimenez, J. L.: Field-Deployable, High-Resolution, Time-of-Flight Aerosol Mass Spectrometer, Anal. Chem., 78, 8281–8289, https://doi.org/10.1021/ac061249n, 2006.
- DiGangi, J. P., Choi, Y., Nowak, J. B., Halliday, H. S., Diskin, G. S., Feng, S., Barkley, Z. R., Lauvaux, T., Pal, S., Davis, K. J., Baier, B. C., and Sweeney, C.: Seasonal Variability in Local Carbon Dioxide Biomass Burning Sources Over Central and Eastern US Using Airborne In Situ Enhancement Ratios, J. Geophys. Res.-Atmos., 126, e2020JD034525, https://doi.org/10.1029/2020JD034525, 2021.
- Diskin, G. S., Podolske, J. R., Sachse, G. W., and Slate, T. A.: Openpath airborne tunable diode laser hygrometer, P. Soc. Photo.-Opt. Ins., 196–204, https://doi.org/10.1117/12.453736, 2002.
- Fleming, Z. L., Monks, P. S., and Manning, A. J.: Review: Untangling the influence of air-mass history in interpreting observed atmospheric composition, J. Atmos. Res., 104–105, 1–39, https://doi.org/10.1016/j.atmosres.2011.09.009, 2012.
- Gelencsér, A., Siszler, K., and Hlavay, J.: Toluene—Benzene Concentration Ratio as a Tool for Characterizing the Distance from Vehicular Emission Sources, Environ. Sci. Technol., 31, 2869—2872, https://doi.org/10.1021/es970004c, 1997.
- Halliday, H. S., DiGangi, J. P., Choi, Y., Diskin, G. S., Pusede, S. E., Rana, M., Nowak, J. B., Knote, C., Ren, X., He, H., Dickerson, R. R., and Li, Z.: Using Short-Term CO/CO₂ Ratios to Assess Air Mass Differences Over the Korean Peninsula During KORUS-AQ, J. Geophys. Res.-Atmos., 124, 10951–10972, https://doi.org/10.1029/2018JD029697, 2019.
- Harris, J. M., Draxler, R. R., and Oltmans, S. J.: Trajectory model sensitivity to differences in input data and vertical transport method, J. Geophys. Res.-Atmos., 110, https://doi.org/10.1029/2004JD005750, 2005.
- Helfter, C., Tremper, A. H., Halios, C. H., Kotthaus, S., Bjorkegren, A., Grimmond, C. S. B., Barlow, J. F., and Nemitz, E.: Spatial and temporal variability of urban fluxes of methane, carbon monoxide and carbon dioxide above London, UK, Atmos. Chem.

- Phys., 16, 10543–10557, https://doi.org/10.5194/acp-16-10543-2016.
- Hilario, M. R. A., Crosbie, E., Shook, M., Reid, J. S., Cambaliza, M. O. L., Simpas, J. B. B., Ziemba, L., DiGangi, J. P., Diskin, G. S., Nguyen, P., Turk, F. J., Winstead, E., Robinson, C. E., Wang, J., Zhang, J., Wang, Y., Yoon, S., Flynn, J., Alvarez, S. L., Behrangi, A., and Sorooshian, A.: Measurement report: Long-range transport patterns into the tropical northwest Pacific during the CAMP2Ex aircraft campaign: chemical composition, size distributions, and the impact of convection, Atmos. Chem. Phys., 21, 3777–3802, https://doi.org/10.5194/acp-21-3777-2021, 2021.
- Hilario, M. R. A., Arellano, A. F., Behrangi, A., Crosbie, E. C., Di-Gangi, J. P., Diskin, G. S., Shook, M. A., Ziemba, L. D., and Sorooshian, A.: Assessing potential indicators of aerosol wet scavenging during long-range transport, Atmos. Meas. Tech., 17, 37–55, https://doi.org/10.5194/amt-17-37-2024, 2024.
- Holloway, T., Levy II, H., and Kasibhatla, P.: Global distribution of carbon monoxide, J. Geophys. Res.-Atmos., 105, 12123–12147, https://doi.org/10.1029/1999JD901173, 2000.
- Khalil, M. A. K. and Rasmussen, R. A.: Carbon Monoxide in the Earth's Atmosphere: Increasing Trend, Science, 224, 54–56, https://doi.org/10.1126/science.224.4644.54, 1984.
- Kondo, Y., Morino, Y., Takegawa, N., Koike, M., Kita, K., Miyazaki, Y., Sachse, G. W., Vay, S. A., Avery, M. A., Flocke, F., Weinheimer, A. J., Eisele, F. L., Zondlo, M. A., Weber, R. J., Singh, H. B., Chen, G., Crawford, J., Blake, D. R., Fuelberg, H. E., Clarke, A. D., Talbot, R. W., Sandholm, S. T., Browell, E. V., Streets, D. G., and Liley, B.: Impacts of biomass burning in Southeast Asia on ozone and reactive nitrogen over the western Pacific in spring, J. Geophys. Res.-Atmos., 109, https://doi.org/10.1029/2003JD004203, 2004.
- Lee, H.-H., Iraqui, O., Gu, Y., Yim, S. H.-L., Chulakadabba, A., Tonks, A. Y.-M., Yang, Z., and Wang, C.: Impacts of air pollutants from fire and non-fire emissions on the regional air quality in Southeast Asia, Atmos. Chem. Phys., 18, 6141–6156, https://doi.org/10.5194/acp-18-6141-2018, 2018.
- Lin, Y. C., Lin, C. Y., Lin, P. H., Engling, G., Lin, Y. C., Lan, Y. Y., June Chang, C. W., Kuo, T. H., Hsu, W. T., and Ting, C. C.: Influence of Southeast Asian biomass burning on ozone and carbon monoxide over subtropical Taiwan, Atmos. Environ., 64, 358– 365, https://doi.org/10.1016/j.atmosenv.2012.09.050, 2013.
- Marvin, M. R., Palmer, P. I., Yao, F., Latif, M. T., and Khan, M. F.: Uncertainties from biomass burning aerosols in air quality models obscure public health impacts in Southeast Asia, Atmos. Chem. Phys., 24, 3699–3715, https://doi.org/10.5194/acp-24-3699-2024, 2024.
- Naik, V., Voulgarakis, A., Fiore, A. M., Horowitz, L. W., Lamarque, J.-F., Lin, M., Prather, M. J., Young, P. J., Bergmann, D., Cameron-Smith, P. J., Cionni, I., Collins, W. J., Dalsøren, S. B., Doherty, R., Eyring, V., Faluvegi, G., Folberth, G. A., Josse, B., Lee, Y. H., MacKenzie, I. A., Nagashima, T., van Noije, T. P. C., Plummer, D. A., Righi, M., Rumbold, S. T., Skeie, R., Shindell, D. T., Stevenson, D. S., Strode, S., Sudo, K., Szopa, S., and Zeng, G.: Preindustrial to present-day changes in tropospheric hydroxyl radical and methane lifetime from the Atmospheric Chemistry and Climate Model Intercomparison Project (ACCMIP), Atmos. Chem. Phys., 13, 5277–5298, https://doi.org/10.5194/acp-13-5277-2013, 2013.

- Nara, H., Tanimoto, H., Tohjima, Y., Mukai, H., Nojiri, Y., and Machida, T.: Emission factors of CO₂, CO and CH₄ from Sumatran peatland fires in 2013 based on shipboard measurements, Tellus B, 69, https://doi.org/10.1080/16000889.2017.1399047, 2017.
- NASA NRT VIIRS FIRMS: 375 m Active Fire product VNP14IMGT, **NASA** Atmospheric Sci-(ASDC) Data Center DAAC [data set], https://doi.org/10.5067/FIRMS/VIIRS/VNP14IMGT_NRT.002, 2020.
- NASA/LARC/SD/ASDC: CAMP2Ex P-3 In-Situ Trace Gas Data, NASA LANCE MODIS at the MODAPS [data set], https://doi.org/10.5067/SUBORBITAL/CAMP2EX2018/DATA001, 2020.
- Pan, L. L., Randel, W. J., Gary, B. L., Mahoney, M. J., and Hintsa, E. J.: Definitions and sharpness of the extratropical tropopause: A trace gas perspective, J. Geophys. Res.-Atmos., 109, https://doi.org/10.1029/2004JD004982, 2004.
- Pan, L. L., Paulik, L. C., Honomichl, S. B., Munchak, L. A., Bian, J., Selkirk, H. B., and Vömel, H.: Identification of the tropical tropopause transition layer using the ozone-water vapor relationship, J. Geophys. Res.-Atmos., 119, 3586–3599, https://doi.org/10.1002/2013JD020558, 2014.
- Plant, G., Kort, E. A., Floerchinger, C., Gvakharia, A., Vimont, I., and Sweeney, C.: Large Fugitive Methane Emissions From Urban Centers Along the U.S. East Coast, Geophys. Res. Lett., 46, 8500–8507, https://doi.org/10.1029/2019GL082635, 2019.
- Plant, G., Kort, E. A., Murray, L. T., Maasakkers, J. D., and Aben, I.: Evaluating urban methane emissions from space using TROPOMI methane and carbon monoxide observations, Remote Sens. Environ., 268, 112756, https://doi.org/10.1016/j.rse.2021.112756, 2022.
- Reid, J. S., Maring, H. B., Narisma, G. T., Heever, S. van den, Girolamo, L. D., Ferrare, R., Lawson, P., Mace, G. G., Simpas, J. B., Tanelli, S., Ziemba, L., Diedenhoven, B. van, Bruintjes, R., Bucholtz, A., Cairns, B., Cambaliza, M. O., Chen, G., Diskin, G. S., Flynn, J. H., Hostetler, C. A., Holz, R. E., Lang, T. J., Schmidt, K. S., Smith, G., Sorooshian, A., Thompson, E. J., Thornhill, K. L., Trepte, C., Wang, J., Woods, S., Yoon, S., Alexandrov, M., Alvarez, S., Amiot, C. G., Bennett, J. R., M., B., Burton, S. P., Cayanan, E., Chen, H., Collow, A., Crosbie, E., DaSilva, A., Di-Gangi, J. P., Flagg, D. D., Freeman, S. W., Fu, D., Fukada, E., Hilario, M. R. A., Hong, Y., Hristova-Veleva, S. M., Kuehn, R., Kowch, R. S., Leung, G. R., Loveridge, J., Meyer, K., Miller, R. M., Montes, M. J., Moum, J. N., Nenes, T., Nesbitt, S. W., Norgren, M., Nowottnick, E. P., Rauber, R. M., Reid, E. A., Rutledge, S., Schlosser, J. S., Sekiyama, T. T., Shook, M. A., Sokolowsky, G. A., Stamnes, S. A., Tanaka, T. Y., Wasilewski, A., Xian, P., Xiao, Q., Xu, Z., and Zavaleta, J.: The coupling between tropical meteorology, aerosol lifecycle, convection, and radiation, during the Cloud, Aerosol and Monsoon Processes Philippines Experiment (CAMP2Ex), B. Am. Meteorol. Soc., 1, E1179-E1205, https://doi.org/10.1175/BAMS-D-21-0285.1, 2023.
- Robinson, N. H., Newton, H. M., Allan, J. D., Irwin, M., Hamilton, J. F., Flynn, M., Bower, K. N., Williams, P. I., Mills, G., Reeves, C. E., McFiggans, G., and Coe, H.: Source attribution of Bornean air masses by back trajectory analysis during the OP3 project, Atmos. Chem. Phys., 11, 9605–9630, https://doi.org/10.5194/acp-11-9605-2011, 2011.

- Rolph, G., Stein, A., and Stunder, B.: Real-time Environmental Applications and Display sYstem: READY, Environ. Modell. Softw., 95, 210–228, https://doi.org/10.1016/j.envsoft.2017.06.025, 2017.
- Silva, S. J., Arellano, A. F., and Worden, H. M.: Toward anthropogenic combustion emission constraints from space-based analysis of urban CO₂/CO sensitivity, Geophys. Res. Lett., 40, 4971– 4976, https://doi.org/10.1002/grl.50954, 2013.
- Smith, M. L., Kort, E. A., Karion, A., Sweeney, C., Herndon, S. C., and Yacovitch, T. I.: Airborne Ethane Observations in the Barnett Shale: Quantification of Ethane Flux and Attribution of Methane Emissions, Environ. Sci. Technol., 49, 8158–8166, https://doi.org/10.1021/acs.est.5b00219, 2015.
- Stein, A. F., Draxler, R. R., Rolph, G. D., Stunder, B. J. B., Cohen, M. D., and Ngan, F.: NOAA's HYSPLIT Atmospheric Transport and Dispersion Modeling System, B. Am. Meteorol. Soc., 96, 2059–2077, https://doi.org/10.1175/BAMS-D-14-00110.1, 2015.
- Voulgarakis, A., Naik, V., Lamarque, J.-F., Shindell, D. T., Young, P. J., Prather, M. J., Wild, O., Field, R. D., Bergmann, D., Cameron-Smith, P., Cionni, I., Collins, W. J., Dalsøren, S. B., Doherty, R. M., Eyring, V., Faluvegi, G., Folberth, G. A., Horowitz, L. W., Josse, B., MacKenzie, I. A., Nagashima, T., Plummer, D. A., Righi, M., Rumbold, S. T., Stevenson, D. S., Strode, S. A., Sudo, K., Szopa, S., and Zeng, G.: Analysis of present day and future OH and methane lifetime in the ACCMIP simulations, Atmos. Chem. Phys., 13, 2563–2587, https://doi.org/10.5194/acp-13-2563-2013, 2013.
- Wei, Y., Shrestha, R., Pal, S., Gerken, T., Feng, S., McNelis, J., Singh, D., Thornton, M. M., Boyer, A. G., Shook, M. A., Chen, G., Baier, B. C., Barkley, Z. R., Barrick, J. D., Bennett, J. R., Browell, E. V., Campbell, J. F., Campbell, L. J., Choi, Y., Collins, J., Dobler, J., Eckl, M., Fiehn, A., Fried, A., Digangi, J. P., Barton-Grimley, R., Halliday, H., Klausner, T., Kooi, S., Kostinek, J., Lauvaux, T., Lin, B., McGill, M. J., Meadows, B., Miles, N. L., Nehrir, A. R., Nowak, J. B., Obland, M., O'Dell, C., Fao, R. M. P., Richardson, S. J., Richter, D., Roiger, A., Sweeney, C., Walega, J., Weibring, P., Williams, C. A., Yang, M. M., Zhou, Y., and Davis, K. J.: Atmospheric Carbon and Transport America (ACT-America) Data Sets: Description, Management, and Delivery, Earth Space Sci., 8, e2020EA001634, https://doi.org/10.1029/2020EA001634, 2021.
- Worden, J. R., Bloom, A. A., Pandey, S., Jiang, Z., Worden, H. M., Walker, T. W., Houweling, S., and Röckmann, T.: Reduced biomass burning emissions reconcile conflicting estimates of the post-2006 atmospheric methane budget, Nat. Commun., 8, 2227, https://doi.org/10.1038/s41467-017-02246-0, 2017.
- Wu, C. and Yu, J. Z.: Evaluation of linear regression techniques for atmospheric applications: the importance of appropriate weighting, Atmos. Meas. Tech., 11, 1233–1250, https://doi.org/10.5194/amt-11-1233-2018, 2018.